Microwave dynamics of gated Al/InAs superconducting nanowires

Applied Physics Letters ARTICLE pubs.aip.org/aip/apl

Microwave dynamics of gated Al/InAs superconducting nanowires

Cite as: Appl. Phys. Lett. **126**, 232602 (2025); doi: 10.1063/5.0267684
Submitted: 25 February 2025 · Accepted: 27 May 2025 ·
Published Online: 10 June 2025

Vittorio Buccheri,[1,a] François Joint,[1,b] Kazi Rafsanjani Amin,[1] Tosson Elalaily,[2,3,4] Olivér Kürtössy,[2,3] Zoltán Scherübl,[2,3] Gergő Fülöp,[2,3] Thomas Kanne,[5] Jesper Nygård,[5] Péter Makk,[2,6] Szabolcs Csonka,[2,3,7] and Simone Gasparinetti[1,c]

AFFILIATIONS

[1]Department of Microtechnology and Nanoscience, Chalmers University of Technology, 41296 Gothenburg, Sweden
[2]Department of Physics, Institute of Physics, Budapest University of Technology and Economics, Műegyetem rkp. 3., H-1111 Budapest, Hungary
[3]MTA-BME Superconducting Nanoelectronics Momentum Research Group, Műegyetem rkp. 3., H-1111 Budapest, Hungary
[4]Low-Temperature Laboratory, Department of Applied Physics, Aalto University School of Science, P.O. Box 15100, FI-00076 Aalto, Finland
[5]Center for Quantum Devices, Niels Bohr Institute, University of Copenhagen, Universitetsparken 5, DK-2100 Copenhagen, Denmark
[6]MTA-BME Correlated van der Waals Structures Momentum Research Group, Műegyetem rkp. 3., H-1111 Budapest, Hungary
[7]Institute of Technical Physics and Materials Science, HUN-REN Centre for Energy Research, Konkoly-Thege Miklós út 29-33, H-1121 Budapest, Hungary

[a]**Author to whom correspondence should be addressed:** buccheri@chalmers.se
[b]**Current address:** Group for Advances Receiver Development (GARD), Department of Space, Earth and Environment, Chalmers University of Technology, 41296 Gothenburg, Sweden.
[c]**Electronic mail:** simoneg@chalmers.se

ABSTRACT

Several experiments have recently reported on gate-tunable superconducting properties in metallic devices, holding promise for the realization of cryogenic switches, tunable resonators, and superconducting logic. In particular, the suppression of the critical current as a function of the gate voltage has been widely investigated. However, time domain studies are discussed only in a few cases. In this paper, we present a microwave characterization of a gate-controlled Al-capped InAs nanowire embedded in a $\lambda/4$ coplanar waveguide resonator. We observe a shift in the resonator frequency and an increase in its internal losses as a function of the gate voltage, which we relate to a change in the imaginary and real components of the nanowire impedance, respectively. We demonstrate that these changes are described by the Mattis–Bardeen model with an effective temperature. We further study the resonator response to fast-varying gate signals and measure characteristic response times of the order of 40 ns, both in time domain and parametric modulation experiments. Our study elucidates the impact of the gate on the complex impedance of the nanowire in the superconducting state, as well as its dynamic performance, providing a foundation for the design of gate-controlled superconducting devices.

Superconductors, thanks to their low energy losses and the Josephson effect, are widely used in cryoelectronics and quantum information processing.[1,2] In these applications, device-design considerations require a specific optimization of superconducting properties such as transition temperature, kinetic inductance, and critical current. For example, kinetic inductance affects the resonant frequency of superconducting resonators,[3] and the spacing of energy levels in transmon qubits depends on the critical current of Josephson junctions.[4]

Although these properties are partially limited by material and geometry,[3] there are strategies to tune them locally and in real time. In superconducting quantum interference devices, for example, a magnetic field is used to control the critical current in one or more Josephson junctions arranged in a superconducting loop.[5,6] On the

other hand, hybrid superconducting-semiconducting systems take advantage of the low carrier density in the semiconducting channel to tune the critical current with an electric field.[7,8]

Recently, several experiments[9–18] have reported electrostatic gate control even in fully superconducting devices. The mechanism behind such findings, which was originally explained as a field effect,[9–11] is still under debate.[14–20] Nonetheless, gate-controlled superconducting devices promise the same flexibility of semiconductor-based technology in terms of local and real-time control. In fact, compared to magnetic field-controlled devices, gate lines are more compact than flux lines and can be designed to affect only a small portion of the sample. Furthermore, both active region and gate can be made of the same metal—the superconductor—which significantly simplifies the fabrication compared to the hybrid semiconducting-superconducting systems. These advantages make gate-controlled superconducting devices appealing for cryoelectronics applications such as superconducting switches,[21] tunable resonators,[22] and fast superconducting electronics.[19,23] A review summarizing the findings, outstanding questions, and possible application of this phenomenon is given in Ref. 24.

One of the systems in which the gate control has been investigated is the indium arsenide (InAs) nanowire with a full-shell of epitaxial aluminum (Al).[17,19] These studies demonstrate the gate effect on highly crystalline superconductors[25] and are valuable for the possible application of the effect in more complex quantum devices. In fact, hybrid Al/InAs nanowires are a promising platform for implementing gatemon[26] and Andreev qubits,[27,28] in which the gate tunability could be an additional experimental control knob. Moreover, a recent experiment[29] on Al/InAs nanowires shows superconducting-normal state switching dynamics on a nanosecond timescale. These findings motivate further investigation of these systems in the microwave regime.

In this paper, we investigate an InAs nanowire—of the same type discussed in Refs. 17, 19, and 29—with the microwave techniques used in Ref. 23. Our device is based on a hybrid semiconducting-superconducting nanowire with impedance Z_{NW}, consisting of a 150 nm diameter InAs core, which is covered with a 20 nm Al full shell [see Fig. 1(a)]. Since the thickness of the Al shell is orders of magnitude larger than the Thomas–Fermi length in Al, the InAs core is screened from the electric field and does not play any role in the gate response of the nanowire,[19] contrary to other configurations.[30] The nanowire is embedded in the current antinode of a $\lambda/4$ coplanar waveguide resonator and gated in a finger-type configuration. The resonator is capacitively coupled to the feedline we use for the readout. We perform our measurements in a dilution cryostat with 10 mK base temperature.

We measure the feedline transmission parameter, S_{21}, with a vector network analyzer (VNA) as a function of the frequency f and DC gate voltage V_g applied to the gate. We observe a dip in $|S_{21}|$, corresponding to the resonator mode, which shifts as a function of V_g [see the heat map in Fig. 1(b)]. In particular, the resonator mode shows a sign-symmetric gate response with an onset around ± 16 V, together with a rise of gate leakage current up to a few nA [see the purple dashed line and the right axis of Fig. 1(a)]. We extract by fit[31] [see supplementary material Figs. S2(b) and S2(c)] resonant frequency f_{res} and internal quality factor Q_i from the resonator trace for each V_g [see Figs. 1(c) and 1(d)]. Both f_{res} and Q_i decrease monotonically, from $f_{res} = 6.84$ GHz and $Q_i = 1000$ at zero gate to $f_{res} = 6.75$ GHz, $Q_i = 100$ around $V_g = \pm 30$ V.

We interpret our result as a consequence of quasiparticle generation in the gated nanowire due to Cooper pair breaking. An increase in the quasiparticle density n_{qp} has a double effect on Z_{NW}: it increases the kinetic inductance L_k, causing a resonant frequency shift, δf_{res}, and introduces a parallel dissipative channel, i.e., a conductance G, which causes an internal quality factor shift, δQ_i.[3] Note that we assume the nanowire fully contributes to the kinetic component of the device inductance [see supplementary material Fig. S2(a)].

By translating the shift in Z_{NW} in terms of a shift in the complex conductivity $\sigma = \sigma_1 + i\sigma_2$, we apply the generalized Mattis–Bardeen model[32,33] and rewrite the shift in f_{res}, Q_i as

$$\frac{\delta f_{res}}{f_{res}} = \frac{\alpha}{2}\frac{\delta \sigma_2}{\sigma_2} \tag{1}$$

and

$$\delta\left(\frac{1}{Q_i}\right) = \alpha\frac{\delta \sigma_1}{\sigma_2}, \tag{2}$$

respectively, where α is the participation ratio between the gate-affected kinetic inductance and the total inductance of the resonator.[22,34,35] A detailed derivation of Eqs. (1) and (2) can be found in Refs. 36 and 37. Here, assuming thermal equilibrium, real and imaginary parts $\sigma_{1,2}$ are functions of temperature T and critical temperature T_c, i.e., $\sigma_i = \sigma_i(T, T_c)$ [supplementary material Eqs. (S1) and (S2)].

In order to obtain T_c and α, we measure δf_{res} and $\delta(1/Q_i)$ in a temperature-driven experiment where $V_g = 0$ V, and the increase in n_{qp} is due to the temperature rise in the cryostat. We fit Eqs. (1) and (2) to our temperature-driven data [see Fig. 1(e)] and obtain $\alpha = 0.14$ and $T_c = 1.31$ K, compatible with aluminum thin films.[38,39]

Then we apply the same model to our gate-driven data, using an effective-temperature approach. The concept of effective temperature is introduced in mesoscopic physics to characterize systems driven out-of-equilibrium.[40–42] This method has been successful in describing the quasiparticles dynamics in superconducting resonators used as kinetic inductance detectors. For example, the effective temperature has been indirectly measured from the quality factor of the resonator[35] or obtained as a fitting parameter of a thermal model.[43] In our case, after obtaining T_c and α from the temperature-driven experiment, we use Eq. (2) to estimate the effective temperature T_{eff} from the measured internal losses $\delta(1/Q_i)$. In turn, by using the obtained α, T_c, and T_{eff}, we find that Eq. (1) describes the gate-driven shift in frequency [see black dashed line following the red data points in Fig. 1(f)], which validates our analysis. Similar experiments about gate-effect on superconductors in the microwave regime are reported in Refs. 16 and 22. However, in Ref. 16, the Mattis–Bardeen model is used to estimate resonator inductance and resistance from material properties, geometry, and temperature, which then feed a simulation that predicts resonant frequency and quality factor. On the other hand, Ref. 22 applies Eqs. (1) and (2) for a remote-gate configuration calculating an effective quasiparticle density and assuming the temperature to be constant. In this case, the model slightly deviates from the experimental data, which the authors attribute to a heating effect.

To summarize this section, the frequency domain characterization of our device shows a gate-driven frequency tunability in excess of 90 MHz, with a contextual $\sim$85% decrease in internal quality factor, both related to a rise in the leakage current from the gate. Furthermore, we can describe the gate-driven relation between δf_{res}

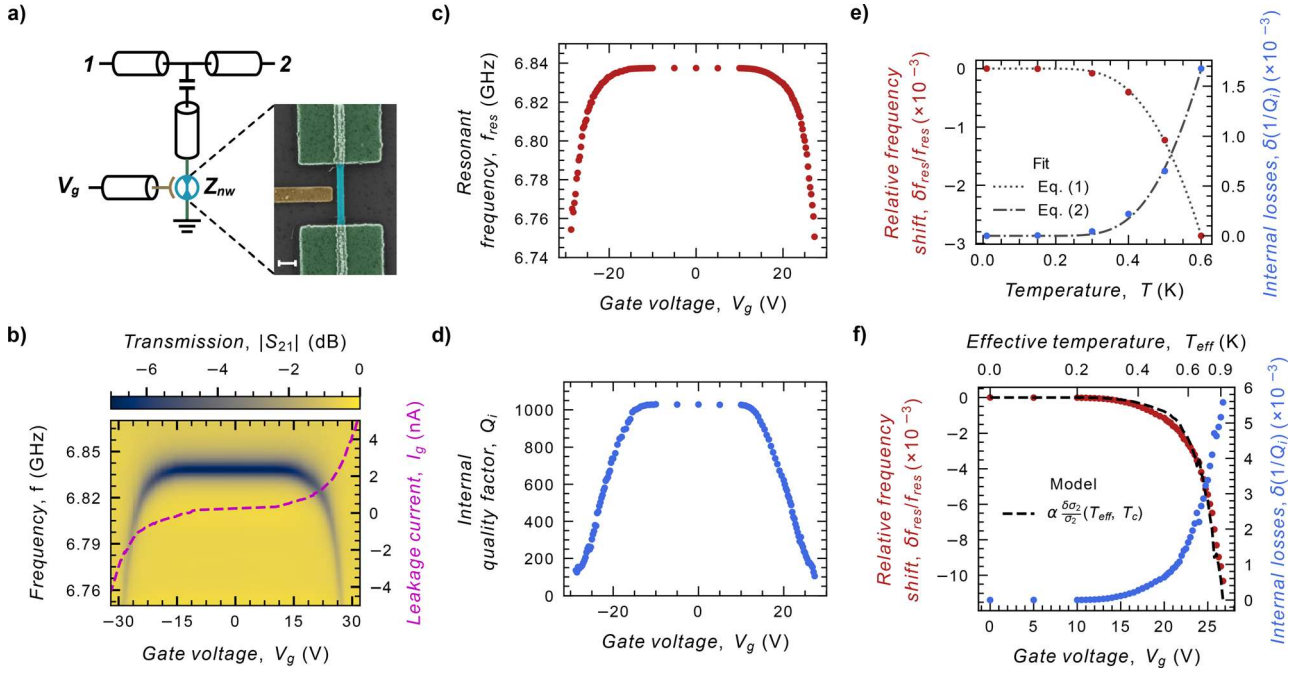

FIG. 1. Device spectroscopy. (a) Simplified schematic of the device. *Zoom-out*: scanning-electron micrograph of the nanowire (scale bar: 300 nm). (b) Heat map of the feedline transmission spectrum, $|S_{21}|$, vs gate voltage, V_g, and frequency, f. On the right axis, we plot the leakage current I_g vs V_g. (c) and (d) Resonant frequency f_{res} and internal quality factor Q_i as a function of V_g. (e) Temperature-driven data with $V_g = 0$: relative frequency shift $\delta f_{res}/f_{res}$ (left axis) and inverse quality factor $\delta(1/Q_i)$ (right axis) are plotted vs temperature. Equations (1) and (2) are globally fitted to the data, according to Mattis–Bardeen model. Fit results: $\alpha = (0.14 \pm 0.04)$ and $T_c = (1.31 \pm 0.05)$ K. (f) Gate-driven data for $T = 10$ mK: $\delta f_{res}/f_{res}$ (left axis) and $\delta(1/Q_i)$ (right axis) vs V_g (bottom axis). For each data point in $\delta(1/Q_i)$, we obtain an effective temperature T_{eff} (top axis), assuming that the gate effect is equivalent to an increase in temperature and using Eq. (2). The predicted $\delta f_{res}/f_{res}$, based on Eq. (1), with the parameter obtained from the fit in panel (e), and $T = T_{eff}$ is plotted as a dashed line.

and $\delta(1/Q_i)$ with an effective temperature in the framework of the Mattis–Bardeen model, which indicates the local heating of the nanowire caused by the leakage current.

We now investigate the dynamic response of our system. We discuss two different techniques for such a measurement: pulsed and continuous gate excitation. In both cases, we send our gate excitation on top of a DC working point V_g, which is above the onset of the gate effect. Excitation and DC signals are combined to the same gate line at the mixing chamber level via a bias-tee [see supplementary material Fig. S6(a)].

Pulsed measurements consist of three pulses: a trigger pulse, a readout pulse, and a gate pulse [see Fig. 2(a)]. We generate all pulses with a microwave digital transceiver, Presto.[44] The trigger pulse defines the time span during which we record the output signal s_{out} from the feedline. While the trigger is on, we send a readout pulse with frequency f_{ro} to the feedline input and a square pulse with amplitude A_g and duration τ_g to the gate line. We average s_{out} over $10^5 - 10^6$ repetition of the triggered sequence and repeat the measurement for different f_{ro}, obtaining a 2D map $s_{out}(t, f_{ro})$ [see Fig. 2(b)].

When $f_{ro} \sim f_{res}$, the readout signal excites the resonator, leaving a signature of the resonant frequency and bandwidth in s_{out}. Consequently, the data at a given time, $s_{out}(t = t_x, f_{ro})$, provides a "snapshot" of the resonator's spectroscopy at time t_x [see $s_{out}(t, f_{ro})$ vertical linecuts on the left side of Fig. 2(c)]. In particular, we fit Lorentzian functions to these frequency traces [see supplementary material Fig. S3(a)], from which we obtain the instantaneous f_{res} and loaded quality factor Q_L. By comparing δf_{res} due to the gate pulse at steady-state with the VNA measurements discussed in the previous section [see left side of Fig. 2(c) vs Fig. 1(c)], we calibrate the attenuation of the RF line we use to drive the gate, obtaining the effective pulse amplitude.

On the other hand, individual time traces $s_{out}(t, f_{ro} \sim f_{res})$ describe the dynamics of our system, namely the resonator ring-up spike around $t = 0.6\,\mu$s and the gate response around $t = 2\,\mu$s [see the $s_{out}(t, f_{ro})$ horizontal linecut on the right side of Fig. 2(c)]. The ring-up decays exponentially to a steady-state level with a characteristic time that defines the resonator response time.[45] From an exponential fit [see supplementary material Fig. S3(b)], we obtain $\tau_{res} = 10$ ns, which is compatible with $Q_L/(2\pi f_{res}) = 16$ ns obtained from the Lorentzian fits.

We then fix $f_{ro} \sim f_{res}$ and choose $A_g = 250$ mV, which induces a variation in $|s_{out}|$ up to a few percents while still leaving the system in the linear response regime. Furthermore, we set $500\,\text{ns} \leq \tau_g \leq 800$ ns, which is long enough to allow $|s_{out}|$ to saturate to a steady value during the pulse excitation but short enough to avoid distortions due to the bias-tee. With these pulse settings, we investigate the characteristic time of the gate response in the resonator time trace as a function of V_g and cryostat base temperature T. In particular, for each V_g or T, we measure the response for both positive and negative pulse ($\pm A_g$). We fit exponential functions to the rising and falling edges of the positive

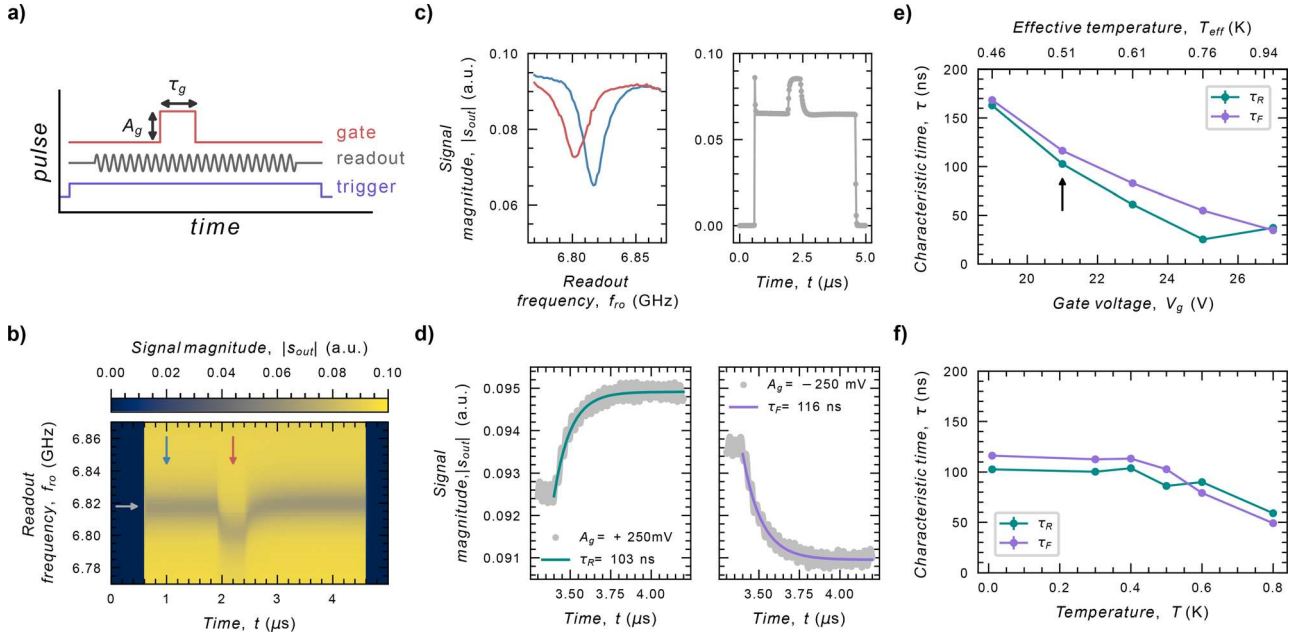

FIG. 2. Device dynamics: time domain spectroscopy. (a) Pulse sequence used for the time-domain measurements. (b) Heat map of resonator time traces recorded for different readout pulse frequencies f_{ro} at gate voltage $V_g = 23.5$ V. With reference to the scheme in panel (a), the trigger period is 5 μs, a 4 μs long readout pulse starts at 0.6 μs and a gate pulse with $A_g = 1.5$ V and $\tau_g = 500$ ns starts around 2 μs. Arrows indicate line cuts discussed in panel (c). (c) Line cuts from panel (b). *Left*: vertical line cuts at 1 μs (blue) and 2.2 μs (red) showing the resonator shift due to the gate pulse. *Right*: horizontal line cut at 6.815 GHz showing resonator ring-up and gate response in time domain. (d) Time traces at $V_g = 21$ V showing resonator rising (left) and falling (right) response under positive and negative gate pulses, respectively. Gate parameters are $|A_g| = 250$ mV and $\tau_g = 800$ ns. Rising (cyan line) and falling (purple line) exponential function are fitted to the gate response, obtaining characteristic time τ_R and τ_F, respectively. (e) Rising and falling time as a function of V_g and effective temperature T_{eff}. The black arrow indicates the gate working point used for the temperature-driven data reported in panel (f). (f) Rising and falling time as a function of the temperature at a fixed $V_g = 21$ V.

and negative pulse-response shape, respectively, obtaining rising and falling characteristic times, $\tau_{R,F}$ [see Fig. 2(d)]. We discard the falling (rising) part of the positive (negative) pulse response, which are affected by the bias-tee in the gate line [see supplementary material Fig. S3(d)].

Since we work in linear regime, we find no clear difference between τ_R and τ_F: they both decrease monotonically with increasing V_g [see Fig. 2(e)], ranging from 170 ns at $V_g = 19$ V to 35 ns at $V_g = 27$ V. We then fix $V_g = 21$ V and measure the characteristic times by stepping the temperature up to 800 mK. We do not observe any clear different behavior between τ_R and τ_F in this case, either: they remain constant at around 130 ns up to 500 mK, then monotonically decrease to 50 ns at 800 mK [see Fig. 2(f)]. Even in time domain, temperature-driven results are compatible with the effective temperature approach. In fact, as discussed in the previous section, $V_g = 21$ V corresponds to $T_{eff} = 510$ mK, which is compatible with the onset in the temperature-induced decrease in $\tau_{R,F}$ for $T \gtrsim 500$ mK.

We compare our data with the expected quasiparticle recombination time, $\tau_{qp} \sim \tau_0/n_{qp}$, where τ_0 is the electron–phonon interaction time in Al.[46] By using the thermal equilibrium $n_{qp}(T_c, T)$, with the critical temperature, T_c, obtained from the temperature-driven frequency spectroscopy, we find that $\tau_0 = 30$ ns leads to a τ_{qp} ranging from 100 ns at $T = 500$ mK to 10 ns at $T = 1$ K (see the supplementary material), which is compatible with the characteristic times we obtain in our experiment as a function of T_{eff}. Whereas τ_0 is often measured to be on the order of 450 ns in aluminum,[46–48] 30 ns is still within the reported range of values for high concentration of aluminum oxide impurities film.[49] On the other hand, also an increase in phonon or quasiparticle density due to nonequilibrium process can effectively decrease τ_0 and τ_{qp}.[46,49,50]

We now perform a continuous gate excitation around $V_g = 27$ V by swapping our pulses with continuous tones. In particular, we send a resonant tone f_r to the feedline input and a tone f_g to the gate, which modulates the device impedance and, consequently, the resonator response. This configuration is equivalent to a mixer where f_r and f_g play the role of local oscillator and intermediate frequency, respectively [see Fig. 3(a)].

We observe sidebands at $f_r \pm f_g$ in the feedline output signal for $f_g = 2$ MHz [see Fig. 3(b)], which proves that f_g modulates f_r. The amplitude of the sideband peaks decreases monotonically with increasing f_g [see Fig. 3(c)]: it ranges from −50 dBm at low frequency to −68 dBm at $f_{g,max} = 25$ MHz with a −3 dB point $f_{g,-3dB} = 3$ MHz, from which we estimate to be an equivalent characteristic response time of $(2\pi f_{g,-3dB})^{-1} = 50$ ns,[51] on the same order of what was obtained in the time domain. Sideband result, which is not limited by bias-tee (bias-tee cutoff is 40 kHz $< f_g$), validates time domain experiments (see the supplementary material for sideband spectroscopy at different V_g and power).

In summary, we discuss the gate response of a Al-capped InAs nanowire embedded in a quarter-wavelength microwave resonator. Spectroscopy characterization of such a system shows a frequency

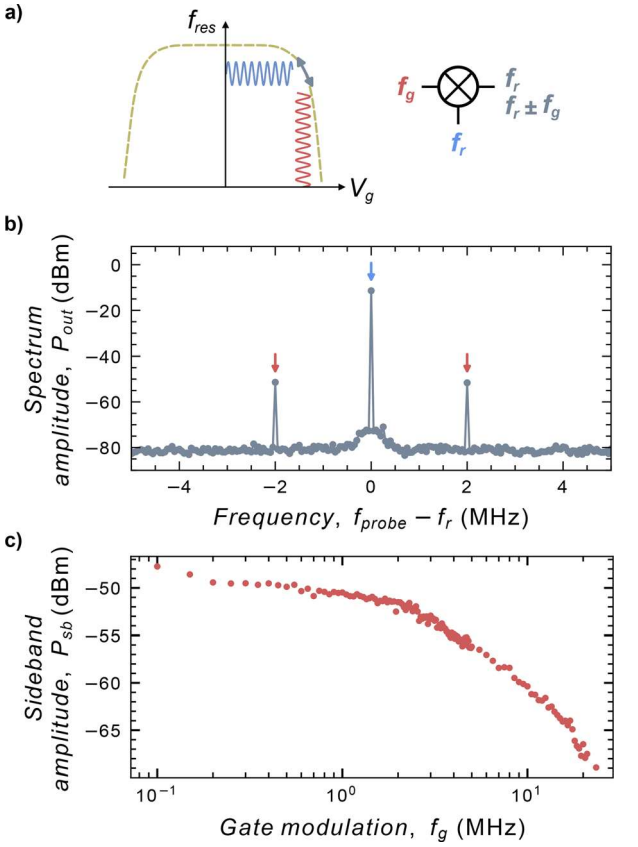

FIG. 3. Device dynamics: sideband spectroscopy. (a) Schematic of the measurement. *Left:* continuous gate excitation modulates the resonator response due to the gate-dependence of the resonator frequency, $f_{res}(V_g)$. *Right:* mixer-equivalent circuit of our system under continuous modulation. (b) Sideband excitation for $V_g = 27$ V, $f_g = 2$ MHz, and $P_g = -5$ dBm. Resonator and sideband peaks are indicated with blue and red arrows, respectively. (c) Averaged upper and lower sideband amplitude [see red arrows in panel (b)] as a function of gate modulation.

tunability on the order of 90 MHz at the price of a degradation in Q_i from 1000 to 100. The onset of the gate response coincides with a rise of the leakage current up to a few nA. We describe the system by the Mattis–Bardeen model with an effective temperature approach, suggesting that the gate response in our device is explained by a heating effect. We note, however, that our use of an effective temperature to model the change in the nanowire impedance does not imply that the quasiparticle population is in thermal equilibrium. In fact, other studies suggest that gating effects on superconductors are related to out-of-equilibrium processes.[14,15,18,19] We study the dynamic response of the resonator under both pulsed and continuous gate excitation. Pulsed excitation is performed in time domain, and it shows a gate-dependent response time down to 35 ns. Even in this experiment, a comparison with temperature-driven measurements suggests that the effect is related to a temperature increase. Continuous excitation confirms the values obtained in time domain, showing sidebands with a −3 dB point at 3 MHz, which gives a characteristic modulation time of 50 ns. Comparison with the expected quasiparticle recombination time suggests that our time domain results agree with the quasiparticle dynamics if we take into account oxygen contamination in our aluminum film or nonequilibrium effects.

Our findings, together with Ref. 23, demonstrate gate-response performances down to tens of nanoseconds, which makes gate-controlled superconducting devices a promising candidate for superconducting switch (see the supplementary material) and cryoelectronics.[24] Moreover, further investigation of the gate dynamics in materials with lower electron–phonon characteristic time and higher critical temperature, such as tantalum (Ta), titanium-nitride (TiN), and niobium-titanium-nitride (NbTiN),[35,46,52,53] could potentially improve the response time.

See the supplementary material for additional information about device fabrication and measurement setup. It also includes supporting data and extended methodologies regarding frequency domain spectroscopy, time domain spectroscopy, and sideband spectroscopy.

The discussed device was partially fabricated in the Chalmers Myfab cleanroom facility. This work was financially supported by the European Research Council via Grant No. 964398 SuperGate, OTKA K138433, ERC project Twistrain, and EIC Pathfinder Challenge QuKiT (No. 101115315). This paper was supported by the János Bolyai Research Scholarship of the Hungarian Academy of Sciences and by the EKÖP-24-4-II-BME-95 University Research Scholarship Program of the Ministry for Culture and Innovation from the source of the National Research, Development, and Innovation Fun. This research was also supported by the Ministry of Culture and Innovation and the National Research, Development and Innovation Office within the Quantum Information National Laboratory of Hungary (Grant No. 2022-2.1.1-NL-2022-00004), and Novo Nordisk Foundation SolidQ. This work was supported by the Knut and Alice Wallenberg Foundation via the Wallenberg Centre for Quantum Technology (WACQT). S.G. acknowledges financial support from the European Research Council via Grant No. 101041744 ESQuAT.

AUTHOR DECLARATIONS

Conflict of Interest

The authors have no conflicts to disclose.

Author Contributions

Vittorio Buccheri: Data curation (equal); Formal analysis (equal); Investigation (equal); Methodology (equal); Software (equal); Visualization (equal); Writing – original draft (equal); Writing – review & editing (equal). **François Joint:** Conceptualization (equal); Methodology (equal); Resources (equal); Writing – review & editing (equal). **Kazi Rafsanjani Amin:** Investigation (supporting); Software (equal). **Tosson Elalaily:** Resources (equal); Writing – review & editing (equal). **Olivér Kürtössy:** Resources (equal). **Zoltán Scherübl:** Supervision (supporting); Writing – review & editing (equal). **Gergő Fülöp:** Supervision (supporting); Writing – review & editing (equal). **Thomas Kanne:** Resources (equal). **Jesper Nygård:** Resources (equal); Writing – review & editing (supporting). **Péter Makk:** Conceptualization (equal); Funding acquisition (equal); Supervision (supporting); Writing – review & editing (equal). **Szabolcs Csonka:** Conceptualization (equal); Funding acquisition (equal); Supervision

(supporting); Writing – review & editing (equal). **Simone Gasparinetti:** Conceptualization (equal); Funding acquisition (equal); Methodology (equal); Project administration (equal); Supervision (equal); Writing – original draft (equal); Writing – review & editing (equal).

DATA AVAILABILITY

The data that support the findings of this study are available from the corresponding author upon reasonable request.

REFERENCES

[1]A. I. Braginski, "Superconductor electronics: Status and outlook," J. Supercond. Nov. Magn. **32**, 23–44 (2019).
[2]M. Kjaergaard, M. E. Schwartz, J. Braumüller *et al.*, "Superconducting qubits: Current state of play," Annu. Rev. Condens. Matter Phys. **11**, 369–395 (2020).
[3]M. Tinkham, *Introduction to Superconductivity*, 2nd ed. (Dover Publication, 2004).
[4]J. Koch, T. M. Yu, J. Gambetta *et al.*, "Charge-insensitive qubit design derived from the Cooper pair box," Phys. Rev. A **76**, 042319 (2007).
[5]R. L. Fagaly, "Superconducting quantum interference device instruments and applications," Rev. Sci. Instrum. **77**, 101101 (2006).
[6]J. Li, P. Barry, T. Cecil *et al.*, "Flux-coupled tunable superconducting resonator," Phys. Rev. Appl. **22**, 014080 (2024).
[7]Y. Chen, D. van Driel, C. Lampadaris *et al.*, "Gate-tunable superconductivity in hybrid InSb–Pb nanowires," Appl. Phys. Lett. **123**, 082601 (2023).
[8]G. Burkard, M. J. Gullans, X. Mi, and J. R. Petta, "Superconductor–semiconductor hybrid-circuit quantum electrodynamics," Nat. Rev. Phys. **2**, 129–140 (2020).
[9]G. De Simoni, F. Paolucci, P. Solinas *et al.*, "Metallic supercurrent field-effect transistor," Nat. Nanotechnol. **13**, 802–805 (2018).
[10]F. Paolucci, G. De Simoni, E. Strambini *et al.*, "Ultra-efficient superconducting Dayem bridge field-effect transistor," Nano Lett. **18**(7), 4195–4199 (2018).
[11]F. Paolucci, F. Vischi, G. De Simoni *et al.*, "Field-effect controllable metallic Josephson interferometer," Nano Lett. **19**(9), 6263–6269 (2019).
[12]C. Puglia, G. De Simoni, and F. Giazotto, "Electrostatic control of phase slips in Ti Josephson nanotransistors," Phys. Rev. Appl. **13**, 054026 (2020).
[13]S. Yu, L. Chen, Y. Pan *et al.*, "Gate-tunable critical current of the three-dimensional niobium nanobridge Josephson junction," Nano Lett. **23**(17), 8043–8049 (2023).
[14]I. Golokolenov, A. Guthrie, S. Kafanov *et al.*, "On the origin of the controversial electrostatic field effect in superconductors," Nat. Commun. **12**, 2747 (2021).
[15]M. F. Ritter, N. Crescini, D. Z. Haxell *et al.*, "Out-of-equilibrium phonons in gated superconducting switches," Nat. Electron. **5**, 71–77 (2022).
[16]G. Catto, W. Liu, S. Kundu *et al.*, "Microwave response of a metallic superconductor subject to a high-voltage gate electrode," Sci. Rep. **12**, 6822 (2022).
[17]T. Elalaily, O. Kürtössy, Z. Scherübl *et al.*, "Gate-controlled supercurrent in epitaxial Al/InAs nanowires," Nano Lett. **21**(22), 9684–9690 (2021).
[18]T. Elalaily, M. Berke, M. Kedves *et al.*, "Signatures of gate-driven out-of-equilibrium superconductivity in Ta/InAs nanowires," ACS Nano **17**(6), 5528–5535 (2023).
[19]T. Elalaily, M. Berke, I. Lija *et al.*, "Switching dynamics in Al/InAs nanowire-based gate-controlled superconducting switch," Nat. Commun. **15**, 9157 (2024).
[20]L. Ruf, T. Elalaily, C. Puglia *et al.*, "Effects of fabrication routes and material parameters on the control of superconducting currents by gate voltage," APL Mater. **11**, 091113 (2023).
[21]M. F. Ritter, A. Fuhrer, D. Z. Haxell *et al.*, "A superconducting switch actuated by injection of high-energy electrons," Nat. Commun. **12**, 1266 (2021).
[22]Y. Ryu, J. Jeong, J. Suh *et al.*, "Utilizing gate-controlled supercurrent for all-metallic tunable superconducting microwave resonators," Nano Lett. **24**(4), 1223–1230 (2024).
[23]F. Joint, K. R. Amin, I. P. C. Cools, and S. Gasparinetti, "Dynamics of gate-controlled superconducting Dayem bridges," Appl. Phys. Lett. **125**, 092602 (2024).
[24]L. Ruf, C. Puglia, T. Elalaily *et al.*, "Gate control of superconducting current: Mechanisms, parameters, and technological potential," Appl. Phys. Rev. **11**, 041314 (2024).
[25]P. Krogstrup, N. L. B. Ziino, W. Chang *et al.*, "Epitaxy of semiconductor–superconductor nanowires," Nat. Mater. **14**, 400–406 (2015).
[26]T. W. Larsen, K. D. Petersson, F. Kuemmeth *et al.*, "Semiconductor-nanowire-based superconducting qubit," Phys. Rev. Lett. **115**, 127001 (2015).
[27]M. Hays, G. de Lange, K. Seriniak *et al.*, "Direct microwave measurement of Andreev-bound-state dynamics in a semiconductor-nanowire Josephson junction," Phys. Rev. Lett. **121**, 047001 (2018).
[28]M. Hays, V. Fatemi, D. Bouman *et al.*, "Coherent manipulation of an Andreev spin qubit," Science **373**, 430–433 (2021).
[29]Z. Scherübl, M. Kocsis, T. Elalalily *et al.*, "Multimode operation of a superconducting nanowire switch in the nanosecond regime," arXiv:2502.17980 (2025).
[30]L. J. Splitthoff, J. J. Wesdorp, M. Pita-Vidal *et al.*, "Gate-tunable kinetic inductance parametric amplifier," Phys. Rev. Appl. **21**, 014052 (2024).
[31]S. Probst, F. B. Song, P. A. Bushev *et al.*, "Efficient and robust analysis of complex scattering data under noise in microwave resonators," Rev. Sci. Instrum. **86**, 024706 (2015).
[32]D. C. Mattis and J. Bardeen, "Theory of the anomalous skin effect in normal and superconducting metals," Phys. Rev. **111**, 412 (1958).
[33]C. S. Owen and D. J. Scalapino, "Superconducting state under the influence of external dynamic pair breaking," Phys. Rev. Lett. **28**, 1559 (1972).
[34]J. Gao, J. Zmuidzinas, A. Vayonakis *et al.*, "Equivalence of the effects on the complex conductivity of superconductor due to temperature change and external pair breaking," J. Low Temp. Phys. **151**, 557–563 (2008).
[35]J. Hu, J. Matin, P. Nicaise *et al.*, "Investigation of quasi-particle relaxation in strongly disordered superconductor resonators," Supercond. Sci. Technol. **37**, 055014 (2024).
[36]P. K. Day, H. G. LeDuc, B. A. Mazin *et al.*, "A broadband superconducting detector suitable for use in large arrays," Nature **425**, 817–821 (2003).
[37]B. A. Mazin, "Microwave kinetic inductance detectors," Ph.D. thesis (California Institute of Technology, 2005).
[38]P. N. Chubov, V. V. Eremenko, and Y. A. Plipenko, "Dependence of the critical temperature and energy gap on the thickness of superconducting aluminum films," Sov. Phys. JETP **28**, 389 (1969).
[39]R. Meservey and P. M. Tedrow, "Properties of very thin aluminum films," J. Appl. Phys. **42**, 51–53 (1971).
[40]V. Chandrasekhar, "Thermal transport in superconductor/normal-metal structures," Supercond. Sci. Technol. **22**, 083001 (2009).
[41]D. Zhang, X. Zheng, and M. Di Ventra, "Local temperatures out of equilibrium," Phys. Rep. **830**, 1–66 (2019).
[42]C. N. Thomas, S. Withington, and D. J. Goldie, "Electrothermal model of kinetic inductance detectors," Supercond. Sci. Technol. **28**, 045012 (2015).
[43]P. P. Budoyo, J. B. Hertzberg, C. J. Ballard *et al.*, "Effects of nonequilibrium quasiparticles in a thin-film superconducting microwave resonator under optical illumination," Phys. Rev. B **93**, 024514 (2016).
[44]M. O. Tholén, R. Borgani, G. R. Di Carlo *et al.*, "Measurement and control of a superconducting quantum processor with a fully integrated radio-frequency system on a chip," Rev. Sci. Instrum. **93**, 104711 (2022).
[45]P. Heidler, C. M. F. Scheider, K. Kustura *et al.*, "Non-Markovian effects of two-level systems in a niobium coaxial resonator with a single-photon lifetime of 10 milliseconds," Phys. Rev. Appl. **16**, 034024 (2021).
[46]P. J. De Visser, "Quasiparticle dynamics in aluminium superconducting microwave resonators," Ph.D. thesis (De Visser, P.J., 2014).
[47]S. B. Kaplan, C. C. Chi, D. N. Langenberg *et al.*, "Quasiparticle and phonon lifetimes in superconductors," Phys. Rev. B **15**, 3567 (1977).
[48]J. M. Martinis, M. Ansmann, and J. Aumentado, "Energy decay in superconducting Josephson-junction qubits from nonequilibrium quasiparticle excitations," Phys. Rev. Lett. **103**, 097002 (2009).
[49]C. C. Chi and J. Clarke, "Quasiparticle branch mixing rates in superconducting aluminum," Phys. Rev. B **19**, 4495 (1979).

[50]D. J. Goldie and S. Withington, "Non-equilibrium superconductivity in quantum-sensing superconducting resonators," Supercond. Sci. Technol. **26**, 015004 (2013).
[51]A. V. Oppenheim and A. S. Willsky, *Signals & Systems*, Signal Processing Series, 2nd ed. (Prentice Hall, 1996), Chap. 6, pp. 448–450.
[52]C. M. Wilson and D. E. Prober, "Quasiparticle number fluctuations in superconductors," Phys. Rev. B **69**, 094524 (2004).
[53]S. A. H. de Rooij, J. J. A. Baselmans, V. Murugesan *et al.*, "Strong reduction of quasiparticle fluctuations in a superconductor due to decoupling of the quasiparticle number and lifetime," Phys. Rev. B **104**, L180506 (2021).